Geophys. J. Int. (2000) **142,** 539–550

Simultaneous waveform inversion for three-dimensional Earth structure and earthquake source parameters considering a wide range of modal coupling

Tatsuhiko Hara[1] and Robert J. Geller[2]

[1] *International Institute of Seismology and Earthquake Engineering, Building Research Institute, Ministry of Construction,* 1 *Tatehara, Tsukuba, Ibaraki,* 305-0802, *Japan. E-mail: thara@kenken.go.jp*

[2] *Department of Earth and Planetary Science, Graduate School of Science, Tokyo University, Hongo* 7-3-1, *Bunkyo-ku, Tokyo* 113-0033, *Japan. E-mail: bob@eps.s.u-tokyo.ac.jp*

Accepted 2000 March 13. Received 1999 December 23; in original form 1998 November 12

SUMMARY

We perform iterative inversion of long-period seismic waveform data to determine simultaneously the 3-D structure of the upper and uppermost lower mantle and earthquake source parameters. We perform direct inversion of the observed data using the methods of Geller & Hara (1993) and Hara (1997), thus intermediate parameters such as 'splitting functions' are not used. We analyse data in the period bands 178–185, 282–299 and 347–376 s using the Direct Solution Method (DSM) to compute synthetic seismograms and their partial derivatives. A wide range of modal coupling is considered in these computations. We conduct numerical experiments that show that neglecting toroidal–spheroidal coupling can significantly bias estimates of 3-D Earth structure for the period band 282–299 s; note that previous studies for this band generally did not consider such coupling. A numerical experiment for the period band 347–376 s suggests that our inversion approach can extract more information on odd angular order structure for the period band 347–376 s than previous techniques.

Key words: Direct Solution Method, lateral heterogeneity, normal modes, surface waves, toroidal–spheroidal coupling, waveform inversion.

1 INTRODUCTION

Accurately determining 3-D seismic Earth structure will contribute to improving our understanding of the dynamics of the Earth's interior. Low-frequency seismic data are useful for this purpose, as they sample the Earth's interior globally and relatively uniformly.

Previous methods for analysing low-frequency seismic data to determine 3-D Earth structure can be divided into two classes. One is the surface wave approach (e.g. Woodhouse & Dziewonski 1984; Zhang & Tanimoto 1993; van Heijst & Woodhouse 1999), and the other is the normal mode approach (e.g. Masters *et al.* 1982; Resovsky & Ritzwoller 1998, 1999). Both methods consider, either explicitly or implicitly, the effect of coupling between different normal mode multiplets due to aspherical structure. In the usual surface wave approach, the local frequency (Jordan 1978) is used to consider the effect of 3-D Earth structure, which is asymptotically equivalent to considering coupling between multiplets on the same branch (Mochizuki 1986; Park 1987; Romanowicz 1987). However, toroidal–spheroidal (T–S) coupling (including the effect of the Earth's rotation) and coupling between multiplets of the same polarization (that is, both spheroidal or both toroidal) on different branches are neglected. In the typical normal mode approach (e.g. Resovsky & Ritzwoller 1998, 1999), coupling between modes on the same branch is neglected in practice (although in principle it could be considered), while other coupling is considered for a small number of multiplets.

The purpose of this paper is to investigate whether neglecting to consider a sufficiently wide range of coupling could significantly bias the 3-D models obtained by inversion for Earth structure. To investigate this question, we carry out full coupling calculations for the period bands 178–185, 282–299 and 347–376 s using the Direct Solution Method (DSM; see Hara *et al.* 1991, 1993; Geller & Ohminato 1994). We use the method of Geller & Hara (1993) for computing the partial derivatives of synthetic seismograms with respect to the parameters of the 3-D earth model and the method of Hara (1997) for CMT inversion.

We briefly summarize the DSM here, as it may not yet be widely familiar. From an algorithmic point of view, the DSM is neither a modal nor a surface wave approach. Mathematically, the DSM falls in the category of Galerkin weak-form methods (see Geller & Ohminato 1994). The solution to the equation

of motion in the frequency domain is expanded in terms of a set of trial functions whose expansion coefficients become the unknowns. This expansion is then substituted into the equation of motion (which is a partial differential equation), and a set of simultaneous linear equations is obtained. The solution of this set of simultaneous linear equations, the vector of expansion coefficients, is then substituted back into the trial function expansion to obtain the synthetic seismograms in the frequency domain. The time-domain synthetics can be obtained by using the inverse DFT (discrete Fourier transform).

The choice of trial functions for the DSM depends on the data being modelled. For long-period multiple surface waves, which are the data considered in this paper, the eigenfunctions of the degenerate singlets of the spherically symmetric part of the model are used as the basis (Hara *et al.* 1991, 1993). As this basis is also used by the modal approach (e.g. Park & Gilbert 1986; Morris *et al.* 1987; Resovsky & Ritzwoller 1998), the DSM synthetics in this study should be essentially equal to the synthetics that would be obtained using the modal approach for the same basis. Thus any differences between the DSM synthetics in this paper and modal synthetics computed in previous studies should be the result of the larger basis used here, which ensures essentially full inclusion of coupling in our synthetics.

For the choice of trial functions used in this study, the system of linear equations solved by the DSM is identical to that solved by frequency-domain modal approaches (e.g. Park & Gilbert 1986; Morris *et al.* 1987). Such modal approaches first determine the eigenfrequencies and eigenfunctions (as well as the dual-space eigenfunctions for non-Hermitian matrices), and then solve the system of linear equations using modal superposition. However, the system of linear equations can also be directly solved without using modal superposition, which is the DSM approach.

The DSM can also be used to compute complete (that is, including both body wave and surface wave) synthetic seismograms (e.g. Takeuchi *et al.* 2000). For either the computation of complete synthetics or the calculations in the present study, the horizontal dependence of the trial functions is given by vector spherical harmonics. However, for the calculation of complete synthetics the vertical dependence of the trial functions is given by linear spline functions rather than the eigenfunctions of the modes of the spherically symmetric model; also, modified operators (Geller & Takeuchi 1995) are used to obtain optimally accurate solutions.

2 INVERSION PROCEDURE

2.1 Model parametrization and unknowns

In the present study, we invert for the 3-D distribution of rigidity in the upper mantle and uppermost lower mantle. In future applications, we plan also to include the 3-D distribution of bulk modulus and density as parameters in our models, either by assuming appropriate proportionality amongst the model parameters or by conducting simultaneous inversion of body wave data (e.g. Takeuchi *et al.* 2000). We divide the model into four layers (11–216, 216–421, 421–671 and 671–888 km), and use a spherical harmonic expansion to represent the lateral variation in each layer. The maximum angular order is $s=8$.

As for the earthquake source parameters, we assume that the trace of the moment tensor is zero. Thus there are nine degrees of freedom for each event (five moment tensor components, the centroid time, depth, latitude and longitude).

2.2 Data

We choose 15 earthquakes that occurred in 1992 and 1993 with moment magnitudes $Mw \geq 7.0$, and analyse the vertical-component records of the VLP (very long period) channel stored in the UVFRAM (ultra and very long-period data in the fast archive recovery method) data set at the IRIS (Incorporated Research Institutions for Seismology) DMC (Data Management Center). The duration of each time series is 9 hr. The total number of seismograms is 402. The present study is preliminary; it will be necessary to enlarge the data set to obtain a more accurate 3-D earth model in future applications.

We choose three period bands for the inversion: 178–185 s, 282–299 s and 347–376 s. We calculate the Fourier spectra of the observed seismograms using the FFT (fast Fourier transform algorithm for computing the DFT) with cosine tapering and conduct deconvolution to remove the instrument response. We use these observed spectra to conduct the inversion in the frequency domain.

2.3 Synthetic seismograms and partial derivatives

We use the DSM to compute synthetic seismograms. We use the eigenfunctions of the degenerate singlets of normal modes computed for model 1066A (Gilbert & Dziewonski 1975) as trial functions. Table 1 shows the multiplets used for each of the above three period bands. In terms of along-branch coupling of fundamental modes, we consider coupling within the angular order range ± 2.

We use the algorithms of Geller & Hara (1993) and Hara (1997) to compute the partial derivatives of synthetic seismograms with respect to the model parameters of the 3-D Earth structure and those of the earthquake source parameters, respectively. The 3-D earth model obtained by each iteration is used as the starting model for the next iteration.

2.4 Initial model

As the initial model we use model 1066A. We include the effect of the Earth's rotation and ellipticity of figure in the potential energy and density matrices, whose definitions are given by Hara *et al.* (1993). We also consider the effect of crustal heterogeneity using the crustal model of Su *et al.* (1994). In future applications, it would be desirable to use a more accurate crustal model such as CRUST 5.1 (Mooney *et al.* 1998). We use the spherically symmetric PREM Q model (Dziewonski & Anderson 1981). We use the earthquake source parameters given by the Harvard catalogue for the initial iteration.

2.5 Inversion scheme

We perform each iteration of the inversion as follows. First, we calculate synthetic spectra using the DSM. We transform the synthetic spectra to the time domain using the FFT. The resulting synthetic seismograms are then tapered and transformed back to the frequency domain, thus yielding processed

Table 1. Multiplets used as trial functions and their eigenperiods for model 1066A.

347–376 s				282–299 s				178–185 s			
${}_0T_{17}$	409.63	${}_0S_{16}$	406.98	${}_0T_{24}$	310.29	${}_0S_{23}$	315.40	${}_0T_{42}$	192.27	${}_0S_{46}$	190.63
${}_0T_{18}$	391.49	${}_0S_{17}$	389.69	${}_0T_{25}$	300.01	${}_0S_{24}$	306.27	${}_0T_{43}$	188.30	${}_0S_{47}$	187.40
${}_0T_{19}$	374.98	${}_0S_{18}$	374.19	${}_0T_{26}$	290.41	${}_0S_{25}$	297.75	${}_0T_{44}$	184.48	${}_0S_{48}$	184.27
${}_0T_{20}$	359.88	${}_0S_{19}$	360.21	${}_0T_{27}$	281.41	${}_0S_{26}$	289.78	${}_0T_{45}$	180.82	${}_0S_{49}$	181.24
${}_0T_{21}$	346.00	${}_0S_{20}$	347.51	${}_0T_{28}$	272.96	${}_0S_{27}$	282.29	${}_0T_{46}$	177.29	${}_0S_{50}$	178.30
${}_0T_{22}$	333.18	${}_0S_{21}$	335.90	${}_0T_{29}$	265.00	${}_0S_{28}$	275.23	${}_0T_{47}$	173.90	${}_0S_{51}$	175.45
${}_0T_{23}$	321.32	${}_0S_{22}$	325.25	${}_1T_{14}$	307.04	${}_0S_{29}$	268.55	${}_0T_{48}$	170.64	${}_0S_{52}$	172.68
${}_1T_9$	407.23	${}_1S_{12}$	391.90	${}_1T_{15}$	293.28	${}_1S_{15}$	315.48	${}_1T_{28}$	190.03	${}_1S_{29}$	190.94
${}_1T_{10}$	381.24	${}_1S_{13}$	362.00	${}_1T_{16}$	280.82	${}_1S_{16}$	299.40	${}_1T_{29}$	185.37	${}_1S_{30}$	185.95
${}_1T_{11}$	358.93	${}_1S_{14}$	336.44	${}_1T_{17}$	269.49	${}_1S_{17}$	286.07	${}_1T_{30}$	180.97	${}_1S_{31}$	181.24
${}_1T_{12}$	339.49	${}_2S_{11}$	388.60	${}_2T_{10}$	305.92	${}_1S_{18}$	274.23	${}_1T_{31}$	176.82	${}_1S_{32}$	176.79
${}_1T_{13}$	322.34	${}_2S_{12}$	365.16	${}_2T_{11}$	289.31	${}_2S_{15}$	308.92	${}_1T_{32}$	172.89	${}_1S_{33}$	172.59
${}_2T_5$	402.16	${}_2S_{13}$	344.72	${}_2T_{12}$	274.31	${}_2S_{16}$	291.01	${}_2T_{21}$	191.81	${}_2S_{25}$	185.86
${}_2T_6$	383.04	${}_2S_{14}$	326.43	${}_3T_1$	311.76	${}_2S_{17}$	274.07	${}_2T_{22}$	186.05	${}_2S_{26}$	179.21
${}_2T_7$	363.18	${}_3S_6$	392.18	${}_3T_2$	308.84	${}_3S_{11}$	310.33	${}_2T_{23}$	180.67	${}_2S_{27}$	174.10
${}_2T_8$	343.29	${}_3S_7$	372.19	${}_3T_3$	304.57	${}_3S_{12}$	297.35	${}_2T_{24}$	175.64	${}_3S_{24}$	190.14
${}_2T_9$	324.03	${}_3S_8$	354.55	${}_3T_4$	299.09	${}_3S_{13}$	285.05	${}_3T_{17}$	190.87	${}_3S_{25}$	184.42
		${}_3S_9$	338.68	${}_3T_5$	292.57	${}_3S_{14}$	273.42	${}_3T_{18}$	184.33	${}_3S_{26}$	178.54
		${}_3S_{10}$	324.05	${}_3T_6$	285.18	${}_4S_8$	290.11	${}_3T_{19}$	178.34	${}_3S_{27}$	171.98
		${}_4S_6$	374.99	${}_3T_7$	277.09	${}_4S_9$	269.53	${}_3T_{20}$	172.84	${}_4S_{20}$	186.25
		${}_4S_7$	326.94	${}_3T_8$	268.48	${}_5S_7$	303.76	${}_4T_{13}$	190.34	${}_4S_{21}$	180.72
		${}_5S_5$	370.07			${}_5S_8$	283.46	${}_4T_{14}$	185.37	${}_4S_{22}$	175.45
		${}_5S_6$	332.17			${}_6S_5$	306.23	${}_4T_{15}$	180.35	${}_5S_{15}$	187.72
		${}_6S_3$	354.60			${}_6S_6$	293.99	${}_4T_{16}$	175.31	${}_5S_{16}$	181.70
		${}_6S_4$	323.59			${}_6S_7$	281.82	${}_5T_1$	186.64	${}_5S_{17}$	176.36
		${}_7S_2$	397.01			${}_6S_8$	267.93	${}_5T_2$	186.05	${}_5S_{18}$	171.46
		${}_7S_3$	320.65			${}_7S_4$	292.91	${}_5T_3$	185.17	${}_6S_{13}$	191.20
		${}_8S_1$	348.32			${}_7S_5$	273.38	${}_5T_4$	184.02	${}_6S_{14}$	184.95
						${}_8S_2$	311.21	${}_5T_5$	182.60	${}_6S_{15}$	178.56
						${}_8S_3$	304.27	${}_5T_6$	180.93	${}_6S_{16}$	172.19
						${}_8S_4$	267.23	${}_5T_7$	179.04	${}_7S_{13}$	186.48
						${}_9S_1$	312.31	${}_5T_8$	176.93	${}_7S_{14}$	174.13
						${}_9S_2$	309.19	${}_5T_9$	174.62	${}_8S_{10}$	181.59
						${}_9S_3$	281.36	${}_5T_{10}$	172.15	${}_8S_{11}$	174.94
										${}_9S_9$	185.65
										${}_9S_{10}$	178.37

synthetic spectra that can be directly compared to the processed observed spectra. We obtain the residuals by subtracting the synthetic spectra from the observed spectra.

We calculate the partial derivatives of the synthetic seismograms with respect to the model parameters of the 3-D model (we follow the same processing steps described above for the synthetics to obtain partials that can be directly compared to the residuals), and invert for the 3-D perturbation to the 3-D starting model. We then conduct CMT inversion using the Green's function computed for the resulting 3-D model.

We iterate the above steps until the changes to the model parameters are sufficiently small. As noted above, the starting model and assumed CMT solutions for the second and later iterations of the inversion are the 3-D model and the CMT solutions obtained by the previous iteration.

We stabilize the solution following Tarantola & Valette (1982). We assume that the *a priori* covariance matrix is diagonal. The assumed initial uncertainty is 0.1 per cent of the spherically symmetric shear wave velocity for each component of the 3-D model parameters, 25 per cent of the maximum value of the initial moment tensor components for each component of the moment tensor (except that for shallow events the uncertainty for $M_{r\theta}$ and $M_{r\phi}$ is reduced to one-tenth), 10 km for depth, 0.1° for the latitude and longitude, and 10 s for the centroid time.

3 RESULTS

3.1 3-D model

Fig. 1 shows the 3-D earth model obtained by five iterations of the above inversion procedure. Although the data set is small, this model shows many features that are known to exist in the upper mantle. For example, in the uppermost layer (11–216 km), there is a good correlation between the lateral heterogeneity and surface tectonics such as high velocities under old continents and low velocities under mid-oceanic ridges (e.g. Woodhouse & Dziewonski 1984). The high velocities under old continents, which correspond to the 'roots' of continents (e.g. Lerner-Lam & Jordan 1987), are still prominent in the second upper layer (216–421 km). The low velocities under mid-oceanic ridges are not significant in this depth range, which suggests that the roots of mid-oceanic ridges are shallow (e.g. Zhang & Tanimoto 1993).

In the transition zone, the most prominent feature is the vast high-velocity region under the western Pacific. This feature persists into the uppermost lower mantle, which suggests that subducting slabs are partially prevented from penetration into the lower mantle (e.g. van der Hilst *et al.* 1991; Fukao *et al.* 1992). The fact that we could obtain this model by analysing

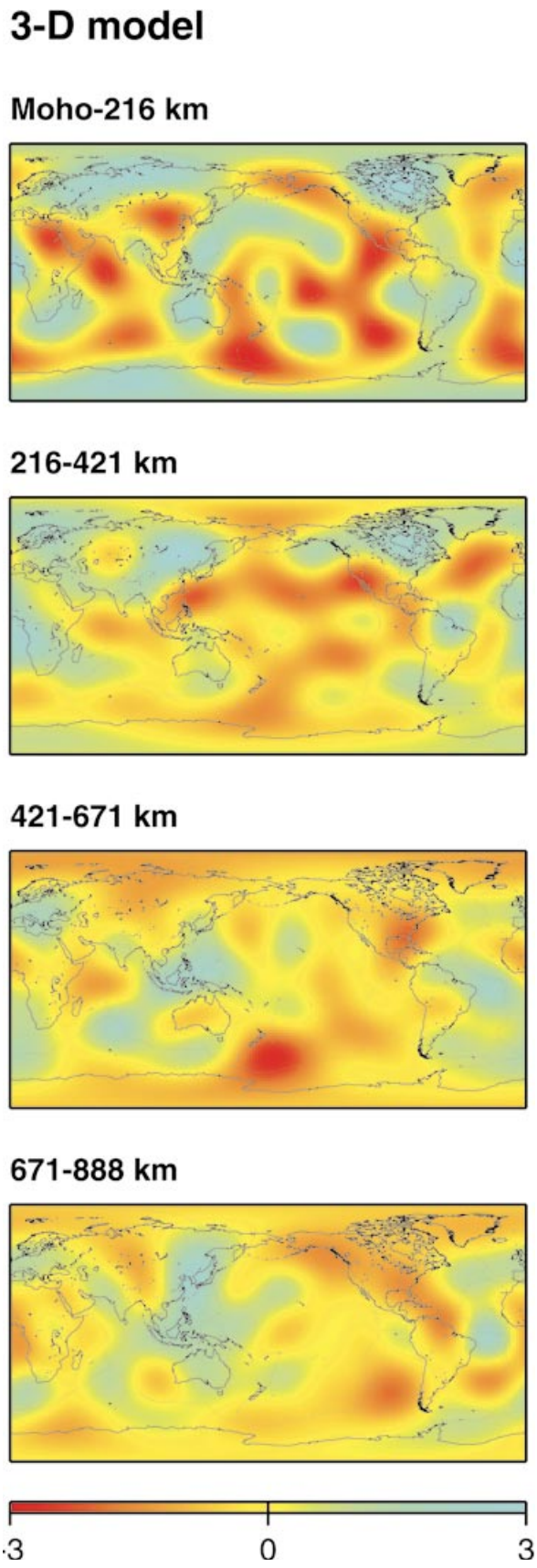

Figure 1. The laterally heterogeneous shear velocity model obtained by our inversion for each depth range. The lateral heterogeneity is specified as a percentage of the spherically symmetric S velocity at the corresponding depth.

a relatively small data set suggests that our technique is promising for future applications, in which a larger data set will be analysed.

3.2 Variance reduction

In Fig. 2, we show the variance reduction obtained by our inversion for each period band. The variance reduction is defined by

$$\text{variance reduction} = \left(1 - \frac{V_{o-c}}{V_o}\right) \times 100 \text{ (per cent)}, \tag{1}$$

where V_o and V_{o-c}, the variance of the observed spectra and that of the residual spectra, respectively, are defined by

$$V_o = \int_{\omega_{min}}^{\omega_{max}} |u_{obs}(\omega)|^2 d\omega, \tag{2}$$

$$V_{o-c} = \int_{\omega_{min}}^{\omega_{max}} |u_{obs}(\omega) - u_{cal}(\omega)|^2 d\omega, \tag{3}$$

where ω is the angular frequency, ω_{max} and ω_{min} are the maximum and minimum angular frequencies for each band, respectively, and u_{obs} and u_{cal} are the observed and synthetic spectra, respectively. We also calculate the variance reduction obtained for the following combinations of earth models and source parameters: (i) model 1066A and the Harvard CMT solutions; (ii) our 3-D model and the Harvard CMT solutions; (iii) our 3-D model and moment tensor solutions and the Harvard centroid location and time (from left to right in Fig. 2). For all three cases, the effects of the Earth's rotation, its ellipticity of figure and crustal heterogeneity are included in the calculation. By comparing the variance reduction for the above three cases to that of our inversion (right-hand side of Fig. 2), we can judge the relative importance of 3-D Earth structure, redetermination of moment tensor and redetermination of centroid location and time in reducing the variance.

In the period band 347–376 s (Fig. 2a), the redetermination of the moment tensor is the largest factor in reducing the variance, 3-D structure is the second largest, and changes of the centroid location and time are the smallest. This suggests the necessity of redetermination of the moment tensor in analysing data in this period band. Fig. 3 shows a comparison of the scalar seismic moment of the best double-couple from the Harvard catalogue and those obtained by the present study. Generally, the scalar seismic moments determined in the present study are larger. Similar results were also obtained by Resovsky & Ritzwoller (1998). In the period band 282–299 s (Fig. 2b), the redetermination of the moment tensor and the 3-D structure have comparable impacts for reducing the variance, while changes of centroid location and time do not have a significant effect. In the period band 178–185 s (Fig. 2c), the 3-D structure is the major factor for reducing the variance, while the remaining two factors have minimal impact.

4 SYNTHETIC TEST INVERSIONS

We conduct the following numerical experiments using synthetic test inversions to investigate the effect of coupling between multiplets on inversion for 3-D Earth structure. In Section 4.1 we investigate the effect of including or neglecting

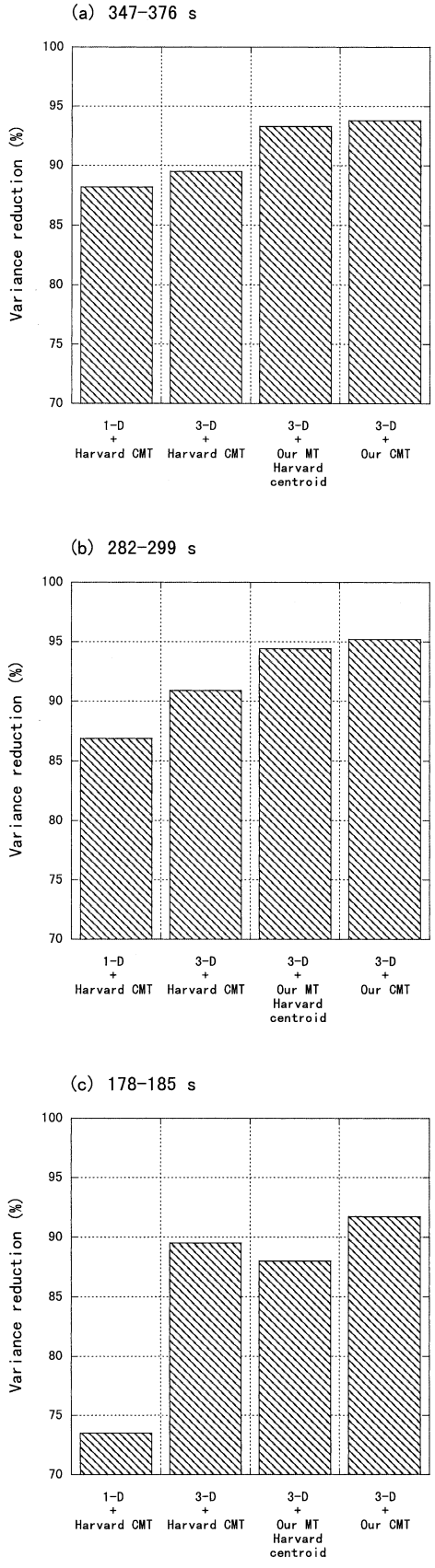

Figure 2. The values of the variance reduction (eq. 1) for the period bands (a) 347–376 s, (b) 282–299 s and (c) 178–185 s. We calculate the variance reduction for four combinations of earth models and source parameters. See the text for details.

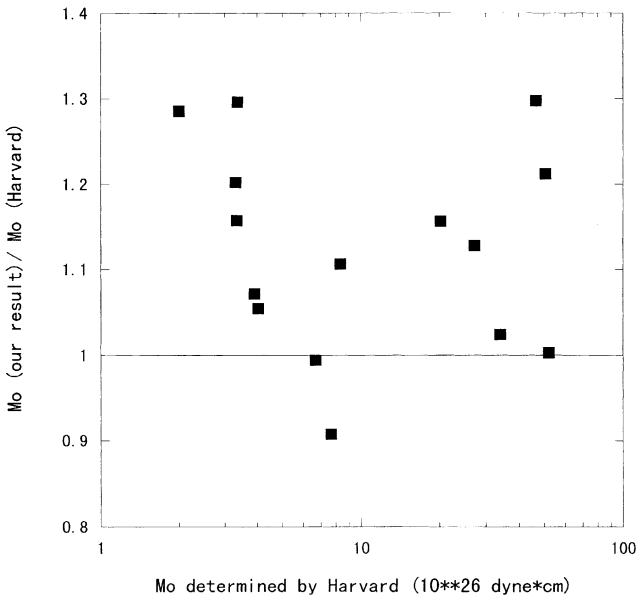

Figure 3. The ratio of the scalar seismic moment of the best double-couple determined by the present study to that of the Harvard catalogue as a function of the latter.

T–S coupling for the three period bands used in the above inversion. In Section 4.2 we compare results in the period band 347–376 s considering all coupling amongst the trial functions to those obtained for the smaller basis used by Resovsky & Ritzwoller (1998, 1999).

4.1 Effect of toroidal–spheroidal coupling

In order to investigate the effect of T–S coupling on inversion for 3-D Earth structure, we compare the results obtained by two analyses for each period band: (i) an analysis that considers the effect of T–S coupling by including the eigenfunctions of both spheroidal and toroidal modes in the basis (Table 1), and (ii) an analysis that neglects the effect of T–S coupling by excluding toroidal trial functions from the basis. Both analyses fully consider all coupling between the trial functions in the respective bases. Thus the second inversion (which neglects T–S coupling) fully considers all coupling between different spheroidal branches.

We conduct numerical experiments as follows. (i) Calculate synthetic seismograms for an assumed 3-D earth model. Note that all coupling for the basis in Table 1 for each respective period range is fully included in the calculation of the synthetics. These synthetics are treated as the 'observed data' in the numerical experiment. (ii) Choose an initial model and perform iterative waveform inversion using the synthetic seismograms calculated in (i) as the 'observed data'. The initial model for the iterative inversion is model 1066A. We use the same events used in Section 3 for these numerical experiments, and select 58 broad-band stations. Thus, the total number of source–receiver paths is 870. The inversion scheme is the same as in Section 3, except that the earthquake source parameters are fixed to the values of the Harvard catalogue. We do not add any noise to the 'observations'.

We choose two models as the 3-D models used to generate the 'observed data' for the inversion experiment. One is a model that has the laterally heterogeneous structure of the 3-D model obtained by the inversion in Section 3 in the depth range 216–421 km and no laterally heterogeneous structure outside this depth range. The other is a model that has the laterally heterogeneous structure of the 3-D model obtained by the inversion in Section 3 in the depth range 421–671 km and no laterally heterogeneous structure outside this range. We use the first model for the period band 178–185 s and the second model for the other two period bands (282–299 s and 347–376 s), since data in the first band and the latter two bands are most sensitive to structure in these respective depth ranges. We do not include the effect of crustal heterogeneity in this numerical experiment.

We first compare the 'observed data' to synthetics for a spherically symmetric model that includes the effect of the Earth's rotation and ellipticity. Fig. 4 shows the variances of the residuals (eq. 3) between the synthetics (for the 1-D model) and the 'observed data' (that is, the synthetics for the 3-D model) specified as a percentage of the variances of the spectra (eq. 2) of the 'observed data' for each band. In making this calculation, $u_{\rm cal}$ is the synthetic calculated for the spherically symmetric model (1066A) and the given basis (with or without T–S coupling), including the effects of rotation and ellipticity. In the period band 347–376 s, the variance when T–S coupling is neglected is over eight times larger than that for synthetics that include T–S coupling. This is an expected result, as it is well known that coupling due to the Coriolis force is significant in this period band (e.g. Masters *et al.* 1983). This result confirms that it is necessary to include the effect of T–S coupling in order to extract information on 3-D Earth structure for this period band. For the period band 282–299 s, the variance obtained without considering T–S coupling is significantly greater (about 30 per cent) than that obtained when T–S coupling is considered, which suggests that T–S coupling should also be considered for this period band. (Note that this is not generally done.) Finally, for the period band 178–185 s the variance with and without considering T–S coupling does not change significantly; thus the effect of T–S coupling is much less significant for this period band.

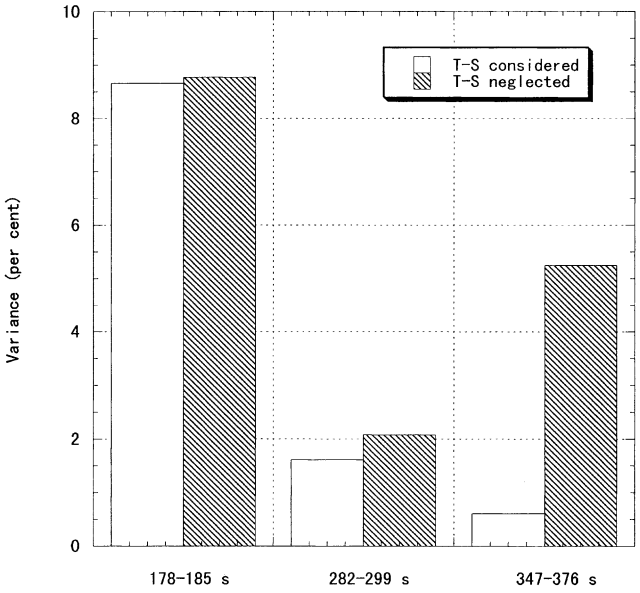

Figure 4. The variances of the residuals (eq. 3) are shown for each period band when synthetics (with and without T–S coupling) for a spherically symmetric model are compared to the synthetics computed for the synthetic 3-D model (including the effect of T–S coupling). The open (left) and hatched (right) bars for each band represent the variance for 1-D synthetics with and without T–S coupling, respectively.

Figs 5(a)–(c) show the 'consistency' between partial derivatives computed for the initial model (1066A) with and without consideration of T–S coupling, which is defined by

'consistency' between partial derivatives for each s

$$= \left(1 - \frac{\dfrac{1}{s} \displaystyle\sum_{t=-s}^{t=s} \int_{\omega_{\min}}^{\omega_{\max}} \left| \left(\frac{\partial u(\omega)}{\partial \mu_s^t} \right)_{\text{with } T\text{–}S} - \left(\frac{\partial u(\omega)}{\partial \mu_s^t} \right)_{\text{without } T\text{–}S} \right|^2 d\omega}{\dfrac{1}{s} \displaystyle\sum_{t=-s}^{t=s} \int_{\omega_{\min}}^{\omega_{\max}} \left| \left(\frac{\partial u(\omega)}{\partial \mu_s^t} \right)_{\text{with } T\text{–}S} \right|^2 d\omega} \right) \times 100 \text{ (per cent)}, \quad (4)$$

where s and t are respectively the angular order and azimuthal order of the spherical harmonics, μ_s^t is the expansion coefficient of the rigidity, and the quantities with the subscripts 'with T–S' and 'without T–S' are calculated with and without consideration of T–S coupling, respectively. Note that in this paper we use s and t to denote the angular order and azimuthal order of the lateral heterogeneity, respectively, and l to denote the angular order of each multiplet in the basis. Figs 5(d)–(f) show the relative values of the denominator of the second term in eq. (4).

In the period band 347–376 s, the values of the consistency for even s structure are less than those for odd s structure (Fig. 5a). This is because, due to the selection rules for matrix elements, fundamental toroidal and spheroidal modes in this band (${}_0S_{18} - {}_0T_{19}$, ${}_0S_{19} - {}_0T_{20}$ and ${}_0S_{20} - {}_0T_{21}$) are coupled through even s structure. The consistency decreases as s increases, because the angular order l of the fundamental mode multiplets becomes comparable to s (Park 1997). In the period band 282–299 s, the values of the consistency are generally larger than those for the period band of 347–376 s (Fig. 5b). In contrast to the period band 347–376 s, the values of the consistency for odd s structure are less than those for even s structure, since fundamental toroidal and spheroidal modes in this band (${}_0S_{25} - {}_0T_{25}$, ${}_0S_{26} - {}_0T_{26}$ and ${}_0S_{27} - {}_0T_{27}$) are coupled through odd s structure. As was also seen for the period band 347–376 s, the consistency for the period band 282–299 s decreases as s increases. For the period band 178–185 s, the values of the consistency are larger than those for the two longer period bands (Fig. 5c), which suggests that the effect of T–S coupling is negligible in this band. This is because s (≤ 8 in this study) is much less than l (~ 50 for the fundamental spheroidal modes in this band) (Park 1997).

The power of the partial derivatives for odd s structure is relatively smaller than that of the partials for even s structure for all three period bands (Figs 5d–f). As shown by Backus (1964), this is due to cancellation of the effect of odd s structure through surface wave propagation on great-circle paths. Hara *et al.* (1993) conducted numerical experiments that fully included all coupling without using great-circle approximations and confirmed that the partial derivatives for odd s structure are considerably smaller than those for even s structure, even when great-circle approximations are not used.

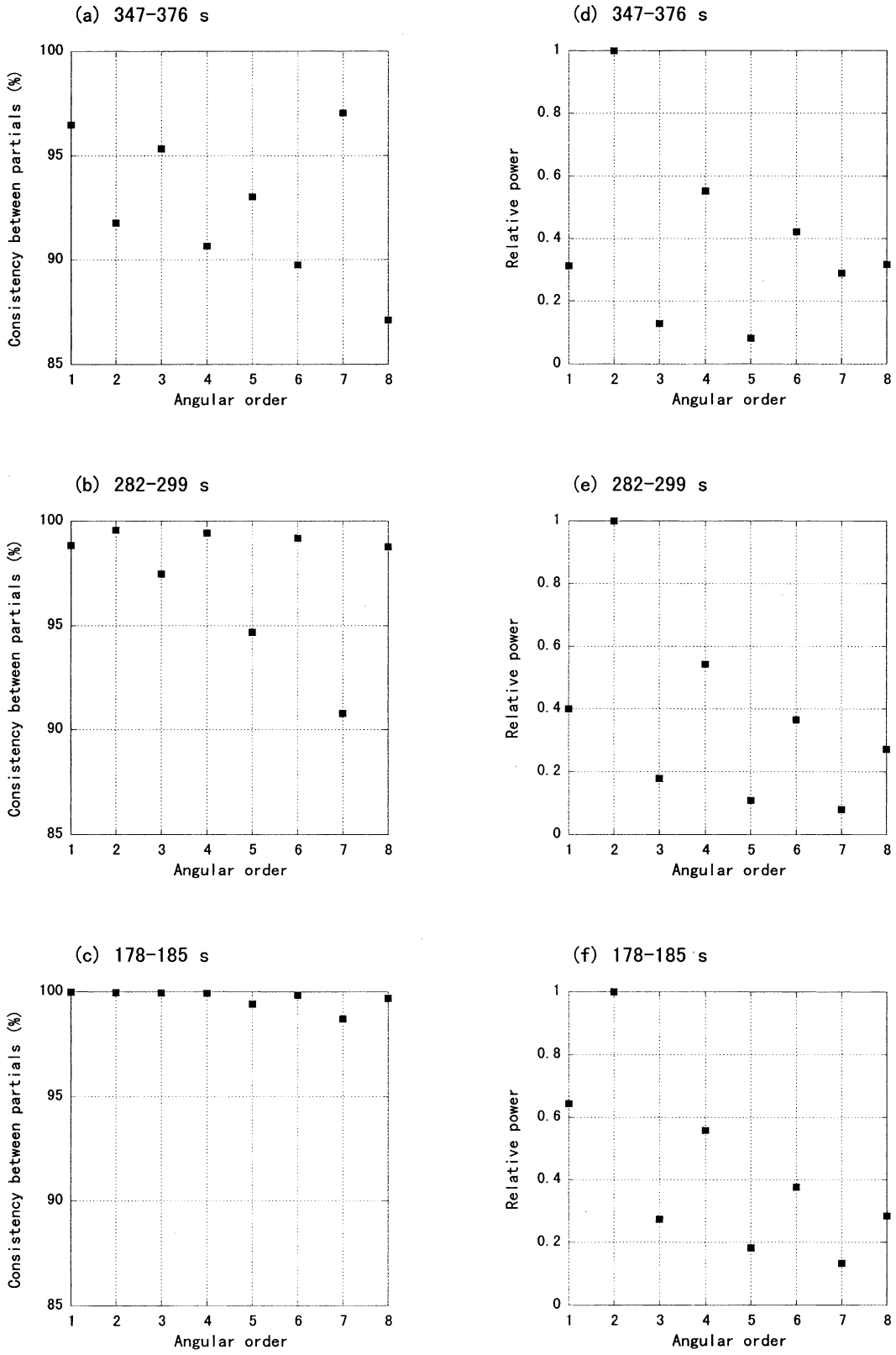

Figure 5. The left panels show the 'consistency' between partial derivatives (eq. 4) for the period bands (a) 347–376 s, (b) 282–299 s and (c) 178–185 s. The right panels (d–f) show the relative power of the partial derivatives (the denominator of the second term in eq. 4) for these period bands.

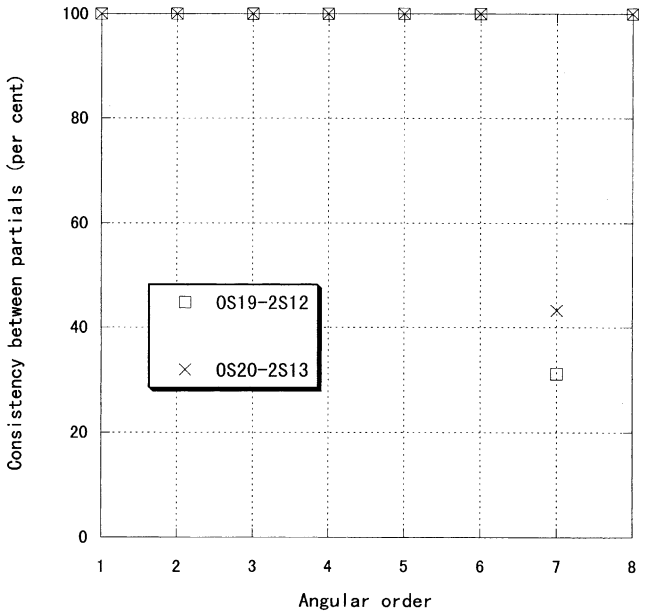

Figure 6. The 'consistency' between the partial derivatives (eq. 4) for two cases: when coupling between ${}_0S_{19}$ and ${}_2S_{12}$ is neglected (open squares) and when coupling between ${}_0S_{20}$ and ${}_2S_{13}$ is neglected (crosses). The value of the 'consistency' is 100 per cent except for $s=7$, since these modes couple through the odd $s(\geq 7)$ structure.

Due to coupling between ${}_0S_{19}-{}_2S_{12}$ and ${}_0S_{20}-{}_2S_{13}$, the relative amplitude for $s=7$ is larger than those for $s=3$ and $s=5$ in the period band 347–376 s (Fig. 5d), despite the fact that the power decreases as s increases. Fig. 6 shows the consistency between the partial derivatives for two cases: in one case coupling of ${}_0S_{19}-{}_2S_{12}$ is neglected and in the other coupling of ${}_0S_{20}-{}_2S_{13}$ is neglected. Note that coupling between these multiplet pairs is not included in the basis used by Resovsky & Ritzwoller (1998, 1999).

Fig. 7 shows results for several inversions of 'observed data'. The 'model consistency', as defined by the following equation, is shown for each angular order s for three period bands:

'model consistency'

$$= \left(1 - \frac{\sum_{t=-s}^{t=s} \int |\mu_s^t(\theta, \phi)_{\text{input}} - \mu_s^t(\theta, \phi)_{\text{output}}|^2 \, d\Omega}{\sum_{t=-s}^{t=s} \int |\mu_s^t(\theta, \phi)_{\text{input}}|^2 \, d\Omega} \right) \times 100 \text{ (per cent)}. \quad (5)$$

Since we do not add any noise to the 'observed data', the input model is almost completely recovered when all coupling is considered (hatched areas in Fig. 7). In contrast, when T–S coupling is omitted from the calculation (open bars in Fig. 7), the model consistency is very small for the period band 347–376 s (Fig. 7a), as the error due to neglecting T–S coupling is very large. For the analysis of data in the period band 282–299 s (Fig. 7b), the model consistency for the inversion omitting T–S coupling is greater than roughly 80 per cent except for $s=4$. Thus the effect of omitting T–S coupling significantly biases the model, although the bias is smaller than for the period band 347–376 s. In both of the above analyses,

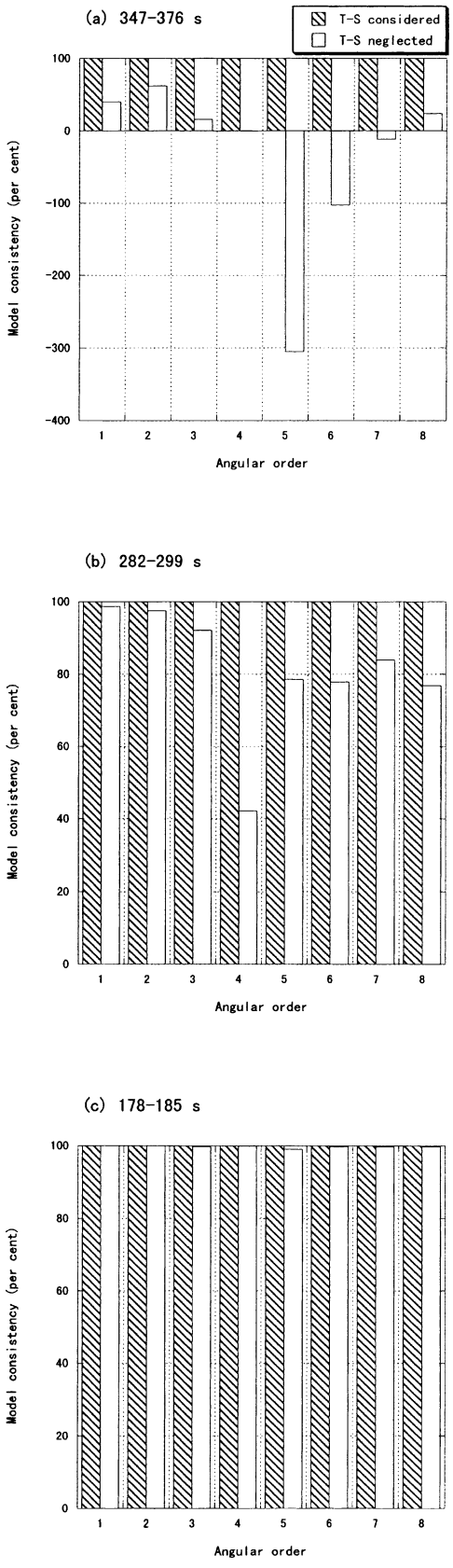

Figure 7. The 'model consistency' (eq. 5) for each angular order s obtained in the numerical experiments for the period bands (a) 347–376 s, (b) 282–299 s and (c) 178–185 s. The left and right columns for each s in each panel show the values obtained with and without consideration of T–S coupling.

there is no systematic difference in the model consistency for odd and even s structure, which is expected based on the results shown in Figs 5(a) and (b). This suggests that the discrepancy between the input and output models is mainly caused by the variances of the residuals shown in Fig. 4, which shows the importance of T–S coupling due to rotation and ellipticity. For the inversion of 'observed data' in the period band 178–185 s, the input model is well recovered by the inversion that omits T–S coupling. This is consistent with the results shown in Figs 4 and 5(c).

Fig. 8 shows the obtained 'variance reduction improvement', defined by

'variance reduction improvement'

$$= \left(1 - \frac{V_{\text{final}}}{V_{\text{initial}}}\right) \times 100 \text{ (per cent)}, \quad (6)$$

where V_{initial} and V_{final} are the variance of the residual spectra (eq. 3) for the initial and final models, respectively. As expected from Fig. 4, the variance reduction is small for the inversion that omits T–S coupling in the period band 347–376 s.

4.2 Comparison to other approaches

Here we conduct an analysis in which only coupling between multiplets considered by Resovsky & Ritzwoller (1998, 1999, hereafter cited as RR in this subsection) is included in the calculation of synthetics. We compare the results of synthetic inversions for this basis to those obtained for inversions using synthetics that include all coupling between the multiplets in Table 1. The 'observed data' are synthetics for the 3-D model that include all coupling. We use the period band 347–376 s; the input model, inversion procedure and source–receiver pairs are the same as in the above numerical experiment.

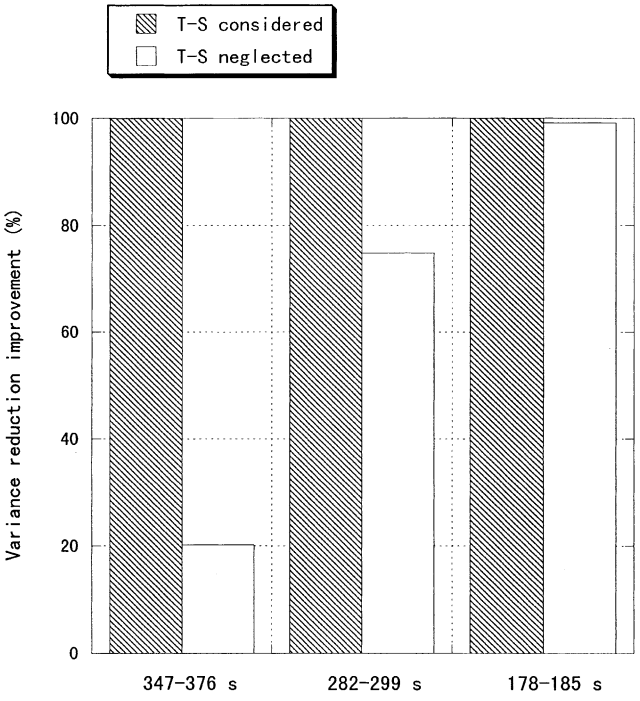

Figure 8. The 'variance reduction improvement' (eq. 6) for each period band. The left and right bars for each angular order s represent the values obtained with and without consideration of T–S coupling.

The duration of the time series is 60 hr, which is a typical value for normal mode analyses. In the inversion approach of RR, a cluster of multiplets such as ${}_6S_3 - {}_3S_8$, whose coupling is considered by RR, must be isolated in the frequency domain by analysing such a very long time series. In contrast, although our approach can also be applied to analyses of such long time series, this is not necessary, as shown above in Section 3, where the length of the time series was 9 hr.

We calculate the 'consistency' between the partial derivatives for the initial model (1066A) using eq. (4) and substituting the partial derivatives computed considering all coupling,

$$(\partial u / \partial \mu_s^l)_{\text{with T–S}},$$

and the partial derivatives computed considering only the coupling included by RR,

$$(\partial u / \partial \mu_s^l)_{\text{without T–S}}$$

(Fig. 9a). Note that we compare the partial derivatives of the synthetic spectra over the entire frequency band used for the inversion. We also show the relative power of the partial derivatives for both calculations (Fig. 9b).

The partial derivatives agree fairly well for even s structure, but do not agree well for odd s structure (Fig. 9a). This is because coupling due to odd s structure is considered by RR only for the pair ${}_6S_3 - {}_3S_8$ in this period band. However, coupling due to odd s structure between multiplets along the same branch and coupling of ${}_0S_{19} - {}_2S_{12}$ and ${}_0S_{20} - {}_2S_{13}$, none of which is considered by RR, makes a significant contribution to the synthetic spectra. Since the pair ${}_6S_3 - {}_3S_8$ does not couple for $s = 1$ and 3, the relative power of the partial derivatives computed considering only this coupling, and thus also the 'consistency' between partial derivatives, is zero for these angular orders (Fig. 9b). The 'consistency' between partial derivatives for $s = 5$ and 7 is not zero, but is very small.

The above results suggest that our inversion approach makes it possible to extract further information on odd s structure than can be obtained by previous approaches. Although the relative power of the partials for odd s structure is smaller than that for even s structure, they are expected to be comparable to those for higher-order even s structure (say $s \sim 12$) based on the trend in Fig. 9. Note that the relative power of the partial derivatives computed considering all coupling for $s = 7$ is larger than those for other odd s structure. This is due to significant coupling between ${}_0S_{19} - {}_2S_{12}$ and ${}_0S_{20} - {}_2S_{13}$, as shown in Section 3 (Fig. 6).

We perform three synthetic inversions: (i) inversion for 3-D structure using the partial derivatives computed considering all coupling, (ii) inversion for only even s structure using the partial derivatives computed considering only the coupling considered by RR, and (iii) inversion for only even s structure using the partial derivatives computed considering all coupling. We do not invert for odd s structure in (ii) because, as mentioned above, the relative power of the partial derivatives for $s = 1$ and 3 is zero, which makes inversion for these angular orders numerically unstable. (In the inversion approach of RR, the isolated cluster of multiplets of ${}_6S_3 - {}_3S_8$ is used for inversion for odd $s \geq 5$ structure, and such instability does not occur.)

Fig. 10 shows the results for the above synthetic inversions. Since we do not add any noise to the 'observed data', the

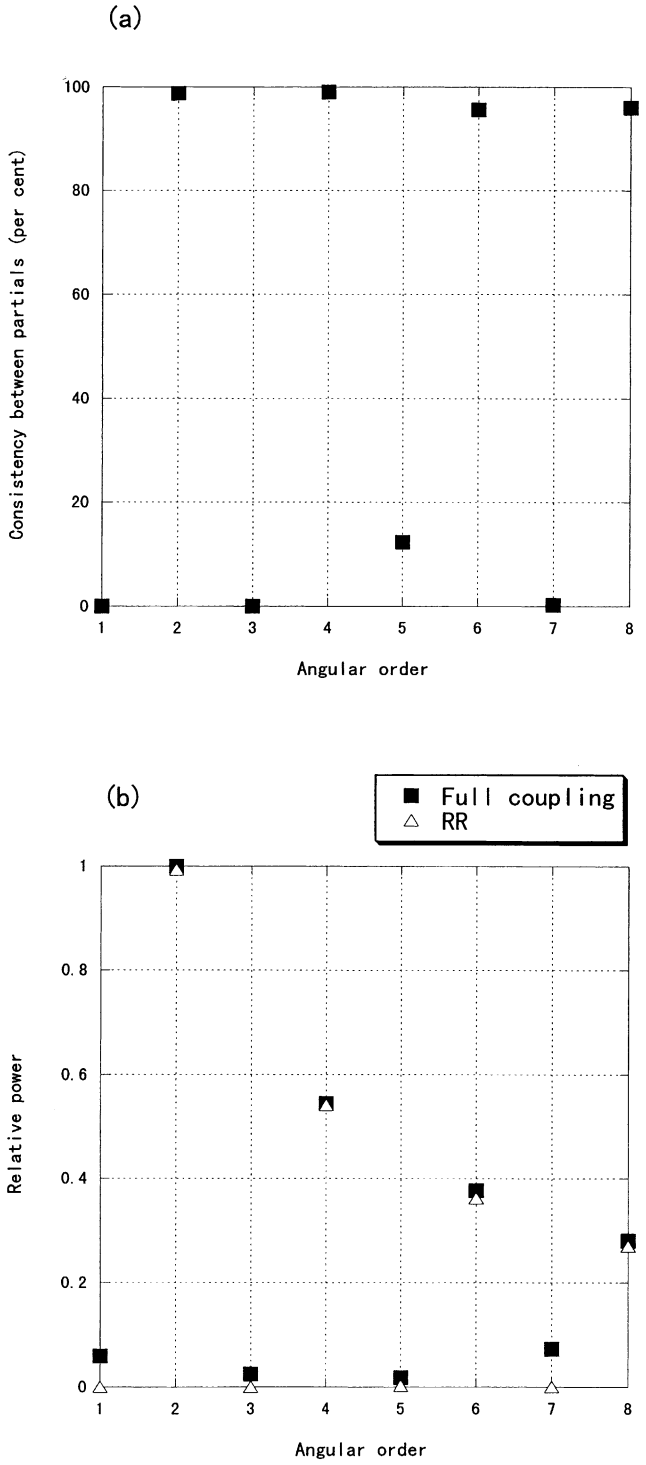

Figure 9. (a) The 'consistency' between the partial derivatives (eq. 4) computed considering all coupling and computed considering only the coupling included by RR. (b) The relative power of the partial derivatives computed considering all coupling (solid squares) and computed considering only the coupling included by RR (open triangles) for each angular order.

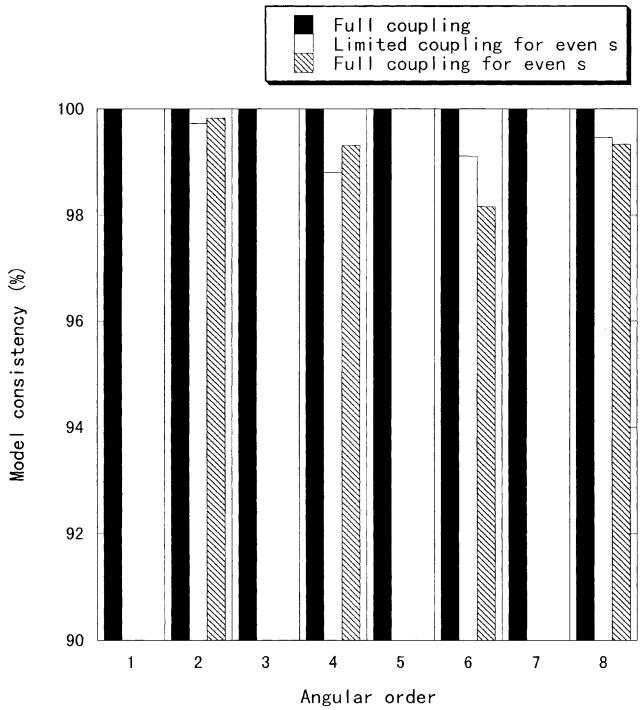

Figure 10. The 'model consistency' (eq. 5) for three inversions. The left column for each angular order is the 'model consistency' for the inversion for all structures considering all coupling; the middle column is that for the inversion for even *s* structure considering only coupling included by RR; the right column is that for the inversion for even *s* structure considering all coupling. The 'model consistency' for odd *s* structure is not shown for the latter two cases.

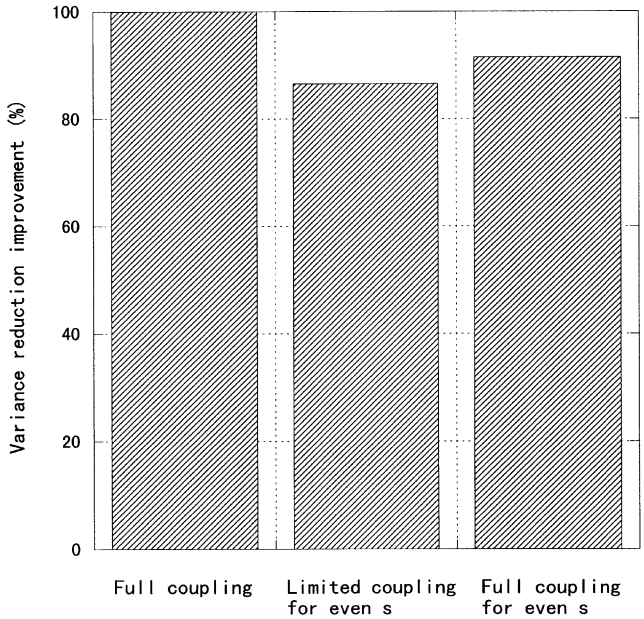

Figure 11. The 'variance reduction improvement' (eq. 6) for three inversions. (Left) the value for the inversion for all structure considering all coupling; (middle) for the inversion for even *s* structure considering only coupling included by RR; (right) for the inversion for even *s* structure considering all coupling.

input model is almost completely recovered by (i). The even *s* lateral heterogeneity is well recovered by (ii) and (iii). Thus, unmodelled odd *s* structure does not significantly affect the estimates of even *s* structure. Fig. 11 shows the variance

reduction improvement (eq. 6) for each of the three synthetic inversions. The variance reduction obtained for (iii) is better than that for (ii).

5 DISCUSSION

In this study, we performed simultaneous waveform inversion for 3-D Earth structure and earthquake source parameters using the DSM to compute synthetics and the inversion algorithms of Geller & Hara (1993) and Hara (1997). We investigated the importance of considering a wide range of modal coupling by conducting numerical experiments. We confirmed the well-known fact that the effect of T–S coupling is particularly important in the period band 347–376 s. Although Resovsky & Ritzwoller (1998, 1999) recently conducted inversion including T–S coupling and coupling for several pairs of multiplets, our numerical experiments show that it is necessary to consider a wider range of coupling in order to obtain accurate information on odd angular order structure. We found that the effect of T–S coupling is also significant in the period band 282–299 s, for which previous analyses have generally neglected T–S coupling. In the period band 178–185 s, the effect of T–S coupling is negligible. Neglecting T–S coupling for the last band makes it possible to reduce significantly the CPU time required for the inversion. However, as shown by Park & Yu (1992) and Yu & Park (1994), this holds only for isotropic models, and it is necessary to include toroidal mode eigenfunctions in the basis when anisotropic structure is being investigated.

Since, as shown in this paper, full-coupling calculations can be carried out in a straightforward manner using the DSM, there is no reason for future studies in long-period seismology to continue to neglect all potentially significant coupling. It appears difficult to extend the surface wave approach to include interbranch and toroidal–spheroidal coupling. On the other hand, the modal approach can in principle easily include all significant coupling simply by enlarging the basis used in the interaction matrix (see e.g. eq. 5 of Resovsky & Ritzwoller 1998). However, application of the inversion approach of Resovsky & Ritzwoller (1998, 1999) to higher frequencies (say higher than 4 mHz) might be difficult, because they first determine structure coefficients (c_s^t in their paper) and then determine 3-D Earth structure by inverting the structure coefficients. Since the number of pairs of multiplets that significantly couple increases with increasing frequency, the number of structure coefficients that must be determined will increase considerably for higher frequencies, which might make their approach impractical.

In contrast, the inversion algorithms of Geller & Hara (1993) and Hara (1997) can readily be applied to higher-frequency data, as structure coefficients are not needed as intermediate results. Note that it is not necessary to compute synthetics using the DSM in order to use these inversion algorithms, which require only that synthetics be calculated accurately for each earthquake source and that back-propagated synthetics be calculated accurately for each receiver component; modal superposition, the DSM or any other accurate approach can equally well be used to compute the synthetics. It appears to us that these inversion algorithms are preferable to the splitting function approach, irrespective of which technique is used to compute the synthetics.

© 2000 RAS, *GJI* **142,** 539–550

ACKNOWLEDGMENTS

We thank Nozomu Takeuchi for comments on an earlier version of this paper, and Daisuke Suetsugu for comments on the present version. We also thank the referees for their comments on an earlier version of this paper. We used HITAC S-3800/480 and MP5800/320 systems at the Computer Center of Tokyo University, NEC SX-4/8 and C4620 systems at the Geographical Survey Institute, and the FUJITSU VX/1R system at the Astronomical Data Analysis Center of the National Astronomical Observatory. This research was partially supported by a grant from the Japanese Ministry of Education, Science, Sports, and Culture (No. 10640403). This research was also partially supported by Special Coordination Funds for promoting Science and Technology of the Science and Technology Agency.

REFERENCES

Backus, G.E., 1964. Geographical interpretation of measurements of average phase velocities of surface waves over great circular and great semi-circular paths, *Bull. seism. Soc. Am.,* **54,** 571–610.

Dziewonski, A.M. & Anderson, D.L., 1981. Preliminary reference Earth model, *Phys. Earth planet. Inter.,* **25,** 297–356.

Fukao, Y., Obayashi, M., Inoue, H. & Nenbai, M., 1992. Subducting slabs stagnant in the mantle transition zone, *J. geophys. Res.,* **97,** 4809–4822.

Geller, R.J. & Hara, T., 1993, Two efficient algorithms for iterative linearized inversion of seismic waveform data, *Geophys. J. Int.,* **115,** 699–710.

Geller, R.J. & Ohminato, T., 1994. Computation of synthetic seismograms and their partial derivatives for heterogeneous media with arbitrary natural boundary conditions using the Direct Solution Method, *Geophys. J. Int.,* **116,** 421–446.

Geller, R.J. & Takeuchi, N., 1995. A new method for computing highly accurate DSM synthetic seismograms, *Geophys. J. Int.,* **123,** 449–470.

Gilbert, F. & Dziewonski, A.M., 1975. An application of normal mode theory to the retrieval of structural parameters and source mechanisms from seismic spectra, *Phil. Trans. R. Soc. Lond.,* A**278,** 187–269.

Hara, T., 1997. Centroid moment tensor inversion of low-frequency seismic spectra using Green's functions for aspherical earth models, *Geophys. J. Int.,* **130,** 251–256.

Hara, T., Tsuboi, S. & Geller, R.J., 1991. Inversion for laterally heterogeneous earth structure using a laterally heterogeneous starting model: preliminary results, *Geophys. J. Int.,* **104,** 523–540.

Hara, T., Tsuboi, S. & Geller, R.J., 1993. Inversion for laterally heterogeneous upper mantle *S*-wave velocity structure using iterative waveform inversion, *Geophys. J. Int.,* **115,** 667–698.

Jordan, T.H., 1978. A procedure for estimating lateral variations from low-frequency eigenspectra data, *Geophys. J. R. astr. Soc.,* **52,** 441–455.

Lerner-Lam, A.L. & Jordan, T.H., 1987. How thick are the continents?, *J. geophys. Res.,* **92,** 14 007–14 026.

Masters, G., Jordan, T.H., Silver, P.G. & Gilbert, F., 1982. Aspherical Earth structure from fundamental spheroidal-mode data, *Nature,* **298,** 609–613.

Masters, G., Park, J. & Gilbert, F., 1983. Observations of coupled spheroidal and toroidal modes, *J. geophys. Res.,* **88,** 10 285–10 298.

Mochizuki, E., 1986. Free oscillations and surface waves of an aspherical earth, *Geophys. Res. Lett.,* **13,** 1478–1481.

Mooney, W.D., Laske, G. & Masters, G., 1998. CRUST 5.1: A global crustal model at $5^\circ \times 5^\circ$, *J. geophys. Res.,* **103,** 727–747.

Morris, S.P., Geller, R.J., Kawakatsu, H. & Tsuboi, S., 1987. Variational free oscillation computations for three laterally heterogeneous earth models, *Phys. Earth planet. Inter.,* **47,** 288–318.

Park, J., 1987. Asymptotic coupled-mode expressions for multiplet amplitude anomalies and frequency shifts on an aspherical earth, *Geophys. J. R. astr. Soc.,* **90,** 129–169.

Park, J., 1997. Free oscillations in an anisotropic earth: path-integral asymptotics, *Geophys. J. Int.,* **129,** 399–411.

Park, J. & Gilbert, F., 1986. Coupled free oscillations of an aspherical, dissipative, rotating earth: Galerkin theory, *J. geophys. Res.,* **91,** 7241–7260.

Park, J. & Yu, Y., 1992. Anisotropy and coupled free oscillations: simplified models and surface wave observations, *Geophys. J. Int.,* **110,** 401–420.

Resovsky, J.S. & Ritzwoller, M.H., 1998. New and refined constraints on three-dimensional Earth structure from normal modes below 3 mHz, *J. geophys. Res.,* **103,** 783–810.

Resovsky, J.S. & Ritzwoller, M.H., 1999. A degree 8 mantle shear velocity model from normal mode observations below 3 mHz, *J. geophys. Res.,* **104,** 993–1014.

Romanowicz, B., 1987. Multiplet-multiplet coupling due to lateral heterogeneity: asymptotic effects on the amplitude and frequency of the earth's normal modes, *Geophys. J. R. astr. Soc.,* **90,** 75–100.

Su, W.-J., Woodward, R.L. & Dziewonski, A.M., 1994. Degree 12 model of shear velocity heterogeneity in the mantle, *J. geophys. Res.,* **99,** 6945–6980.

Takeuchi, N., Geller, R.J. & Cummins, P.R., 2000. Complete synthetic seismograms for 3-D heterogeneous Earth models computed using modified DSM operators and their applicability to inversion for Earth structure, *Phys. Earth planet. Inter.,* **119,** 25–36.

Tarantola, A. & Valette, B., 1982. Generalized nonlinear inverse problems solved using the least squares criterion, *Rev. Geophys. Space Phys.,* **20,** 219–232.

van der Hilst, R.D., Engdahl, E.R., Spakman, W. & Nolet, G., 1991. Tomographic imaging of subducted lithosphere below northwest Pacific island arcs, *Nature,* **353,** 37–43.

van Heijst, H.J. & Woodhouse, J., 1999. Global high-resolution phase velocity distributions of overtone and fundamental-mode surface waves determined by mode branch stripping, *Geophys. J. Int.,* **137,** 601–620.

Woodhouse, J.H. & Dziewonski, A.M., 1984. Mapping the upper mantle: three-dimensional modeling of Earth structure by inversion of seismic waveforms, *J. geophys. Res.,* **89,** 5953–5986.

Yu, Y. & Park, J., 1994. Hunting for azimuthal anisotropy beneath the Pacific Ocean region, *J. geophys. Res.,* **99,** 15 399–15 421.

Zhang, Y.-S. & Tanimoto, T., 1993. High-resolution global upper mantle structure and plate tectonics, *J. geophys. Res.,* **98,** 9793–9823.